Quantum Hall Effect of Dirac Fermions in Graphene: Disorder Effect and Phase Diagram

D. N. Sheng[1], L. Sheng[2] and Z. Y. Weng[3]

[1]*Department of Physics and Astronomy, California State University, Northridge, California 91330*
[2]*Department of Physics and Texas Center for Superconductivity, University of Houston, Houston, Texas 77204*
[3]*Center for Advanced Study, Tsinghua University, Beijing 100084, China*

We numerically study the interplay of band structure, topological invariant and disorder effect in two-dimensional electron system of graphene in a magnetic field. Two *distinct* quantum Hall effect (QHE) regimes exist in the energy band with the unconventional "half-integer" QHE appearing near the band center, consistent with the experimental observation. The latter is more robust against disorder scattering than the conventional QHE states near the band edges. The phase diagram for the unconventional QHE is obtained where the destruction of the Hall plateaus at strong disorder is through the float-up of extended levels toward band center and higher plateaus always disappear first. We further predict a new insulating phase between $\nu = \pm 2$ QHE states at the band center, which may explain the experimentally observed resistance discontinuity near zero gate voltage.

With the advances in micromechanical extraction and fabrication techniques, high mobility single atomic layer of graphite, called graphene, became available recently [1, 2, 3, 4], which has attracted much experimental and theoretical interest. This new material has many extraordinary properties such as submicron-scale ballistic transport at room temperature, ability to sustain high electric currents, and ease of tuning carrier density for both electrons and holes. It is generally believed that graphene may have potential applications in electronic devices [1, 2, 3, 4]. Graphene is of great fundamental interest as well because of its special band structure [5]. Undoped graphene has one π electron per lattice site forming a two-dimensional (2D) extended electronic structure. The only states at the Fermi energy ($E_F = 0$) are at two corners of the Brillouin zone, where the conduction and valence bands touch. The low energy excitations have a linear dispersion relation similar to that of the massless Dirac equation, where the electron Fermi velocity plays the role of an effective "speed of light". So the electron system of graphene can be viewed as a condensed-matter realization of relativistic Dirac fermions, and the band touching points are often referred to as Dirac points.

Remarkably, novel quantum Hall effect (QHE) with Hall plateaus obeying the unconventional quantization rule $\sigma_{xy} = (k + 1/2)g_s \frac{e^2}{h}$ has recently been observed experimentally [6, 7] in graphene films in a strong magnetic field. Here, k is an integer and $g_s = 4$ stands for the spin and sublattice-related degeneracy. In units of $g_s \frac{e^2}{h}$, the "half-integer" quantization of σ_{xy} was conjectured to be due to the nontrivial Berry phase of the Dirac fermions in a magnetic field [6, 7, 8]. Interestingly, calculations [9, 10, 11, 12] by using an analogy to the $2+1$ dimensional Quantum Electro Dynamics have predicted a "half-integer" quantized QHE for graphene. Disorder effect has been studied by using self-consistent Born ap-

proximation within the continuous model [12]. However, so far the interplay of the band structure, particle-hole symmetry, disorder effect, and topological property of the energy band in the unconventional QHE has not yet been investigated. It is thus highly desirable to perform exact numerical calculations by taking into account the full band structure and random disorder, in order to reveal the fundamental nature of the new QHE phases and related quantum phase transitions in graphene.

In this Letter, we study the QHE in graphene using a tight-binding model. The experimentally observed unconventional Hall plateaus are reproduced around the band center $E_F = 0$, while the conventional integer QHE plateaus appear near the band edges. The unusual distribution of the topological invariant quantity-Chern number in the energy band and the conservation of total Chern number (which is also the geometric Berry phase [13]) for the particle and hole bands account for the unconventional "half-integer" QHE. The latter is found to be much more stable than the conventional ones near the band edges against disorder scattering. We map out the whole phase diagram for the QHE and demonstrate that the QHE plateaus are destroyed at strong disorder (or weak magnetic field) through the float-up of extended levels toward the band center. We further identify a new insulating phase between $\nu = \pm 2$ QHE states, which may explain the experimentally observed discontinuity in resistance[6, 7] near zero gate voltage.

We consider a rectangular sample of 2D graphene sheet consisting of carbon atoms on a honeycomb lattice [5, 14], which has totally L_y zigzag chains with L_x atomic sites on each chain [14]. The size of the sample will be denoted as $L_x \times L_y$. In the presence of an applied magnetic field perpendicular to the graphene plane, the lattice model
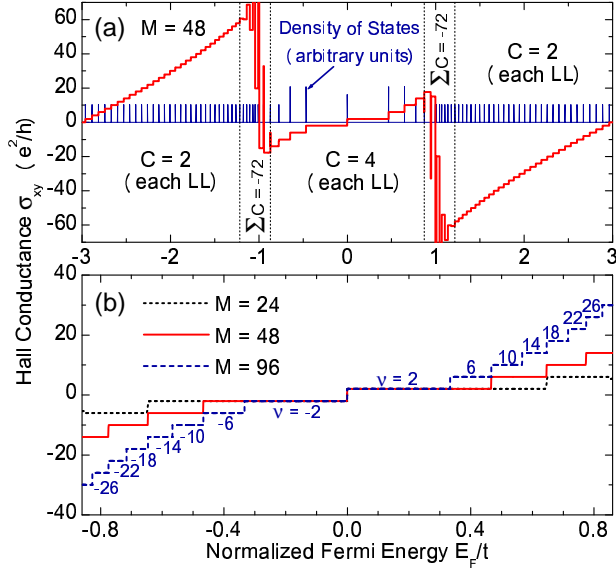
FIG. 1: (a) Calculated Hall conductance and electron density of states in the full energy band for magnetic flux strength $\phi = \frac{2\pi}{48}$ or $M = 48$, and (b) the unconventional Hall conductance for three different strengths of magnetic flux near the band center. Here the disorder strength is set to $W = 0$ and the sample size is taken to be 96×48.

can be written in the tight-binding form [5, 15]:

$$ H = -t \sum_{\langle ij \rangle \sigma} e^{ia_{ij}} c_{i\sigma}^{\dagger} c_{j\sigma} + \sum_{i} w_i c_{i\sigma}^{\dagger} c_{i\sigma} \ , \qquad (1) $$

where $c_{i\sigma}^{+}$ $(c_{i\sigma})$ creates (annihilates) a π electron of spin σ on lattice site i with t as the nearest-neighbor hopping integral, and w_i is random disorder potential uniformly distributed in the interval $w_i \in [-W/2, W/2]$. The magnetic flux per hexagon $\phi = \sum_{\hexagon} a_{ij} = \frac{2\pi}{M}$ is proportional to the strength of the applied magnetic field B. This tight-binding model is valid for describing the full energy band and realizes the energy dispersion relation of the Dirac fermions near the band center [5].

The Hall conductance σ_{xy} can be calculated by using the Kubo formula through exact diagonalization of the system Hamiltonian [15]. In Fig. 1a, the Hall conductance σ_{xy} and electron density of states are plotted as functions of electron Fermi energy E_F for a clean sample $W = 0$ with magnetic flux $\phi = \frac{2\pi}{48}$, which illustrates the overall picture of the QHE in the full energy band. According to the behavior of σ_{xy}, the energy band is naturally divided into three different regimes. Around the band center, $\sigma_{xy} = \nu \frac{e^2}{h}$ is indeed quantized according to the unconventional quantization rule $\nu = (k+1/2)g_s$ with a degeneracy factor $g_s = 4$ for each Landau level (LL) due to two spin directions and two Dirac points. These Hall plateaus explain the experimentally observed unconventional QHE [6, 7] and agree with the results from the theory based upon the continuous model [9, 10, 11, 12]. In Fig. 1b, the Hall conductance in this unconventional

region for three different strengths of magnetic flux is shown. With decreasing magnetic flux from $\phi = \frac{2\pi}{24}$ to $\phi = \frac{2\pi}{96}$, more quantized Hall plateaus emerge following the same quantization rule. We see that the widths of the plateaus are roughly proportional to $\sqrt{\phi} \propto \sqrt{B}$, in agreement with the continuous theory [9, 10]. The unconventional QHE in the present band model can be understood in terms of the topological invariant Chern number [15, 16]. Inside each LL, there are extended states characterized by a nonzero Chern integer. The total Hall conductance in units of $\frac{e^2}{h}$ is exactly the sum of the Chern numbers of all the occupied extended states [15, 16]. The additional degeneracy $g_s = 4$ around the band center gives rise to a total Chern number $C = 4$ for each LL. Thus when each additional LL is occupied, the Hall conductance increments by $g_s \frac{e^2}{h}$. At the particle-hole symmetric point $E_F = 0$, corresponding to the half-filling of the central LL, $\sigma_{xy} = 0$ and the total Chern number of all the occupied states (hole band) must sum up to zero. Now one can count σ_{xy} from this point, and find that the central LL effectively contributes $\pm (\frac{g_s}{2}) \frac{e^2}{h}$ to σ_{xy}, when E_F is shifted away from the central LL by adding particles or holes. This leads to the experimental "half-integer" quantization of σ_{xy} in units of $g_s \frac{e^2}{h}$. As will be shown below, the total zero Chern number for the particle or hole band resulting from the particle-hole symmetry in the pure system remains to be true in the presence of disorder.

Near the band edges, each LL carries a total Chern number $C = 2$, and thus the Hall conductance is quantized as $\sigma_{xy} = kg_s \frac{e^2}{h}$ with k an integer and $g_s = 2$ for spin degeneracy only, which is as same as that in the conventional QHE systems. Remarkably, around $E_F = \pm t$, there are two new critical regions, which separate the unconventional and conventional QHE states. The extended states in each critical region carry a large negative total Chern number, e.g., $\sum C = -72$ for $\phi = \frac{2\pi}{48}$, as shown in Fig. 1a. The existence of the negative Chern number regimes around $E_F = \pm t$ is crucial for understanding the behavior of the Hall conductance in the whole energy band. When the Fermi energy E_F is increased from the band bottom toward band center continuously, following a whole sequence of the conventional Hall plateaus, the negative Chern numbers cause a dramatic reduction and a sign inversion of σ_{xy}, so that the unconventional low Hall plateaus with $\nu = -6, -2, 2 \cdots$ can reoccur near the band center. This is in contrast to the QHE on a square lattice, where stable Hall plateaus can only be observed near the band edges [15].

We have shown that the unconventionally quantized QHE observed in the experiments can be reproduced in the lattice model, and is due to the unusual topological property of the energy band. We next turn to the effect of random disorder on the QHE. In Fig. 2, the Hall conductance around the band center is shown as a function
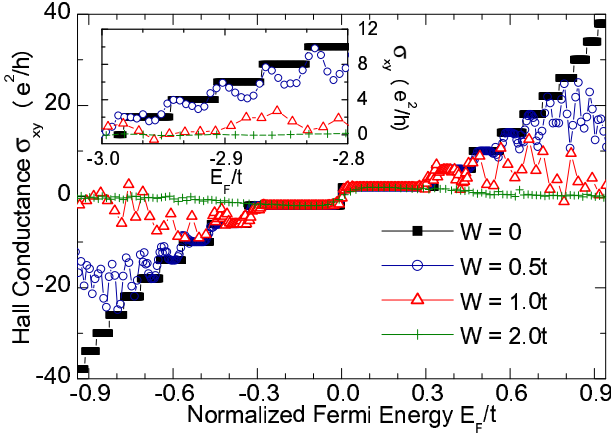
FIG. 2: Unconventional Hall conductance as a function of electron Fermi energy near the band center for four different disorder strengths each averaged over 200 disorder configurations. Inset: conventional Hall conductance near the lower band edge. Here $M = 96$ and the sample size is 96×48.

of E_F for magnetic flux $\phi = \frac{2\pi}{96}$ and four different values of disorder strength W. We see that with increasing W, higher Hall plateaus (with larger $|\nu|$) are destroyed first. At $W = 0.5t$, the plateaus with $\nu = \pm 10, \pm 6$ and ± 2 remain well quantized, while at $W = 2.0t$ all the plateaus except for the $\nu = \pm 2$ ones are destroyed. These last two plateaus will eventually disappear at $W \sim 2.5t$. For comparison, the QHE near the lower band edge is shown in the inset, where all plateaus are found to be destroyed at a much weaker disorder $W = 1.0t$. This clearly indicates that, under the same conditions, the unconventional QHE is much more stable than the conventional one. This is attributed to the Dirac-fermion-like linear dispersion relation around the band center, where the widths of the LL gaps are proportional to $\sqrt{B}$ instead of B. We also notice that, σ_{xy} always vanishes at $E_F = 0$ for all W, due to the fact that the whole particle or hole band carries zero total Chern number as a topological invariant in the disordered system.

We further study the quantum phase transition of the graphene electron system and establish the phase diagram for the QHE. This can be done relatively conveniently by calculation of the finite-size localization length λ on an essentially infinitely long bar of width L_y (length $L_x \geq 10^6$) by using the well-established recursive Green's function approach [17]. We present the calculated phase diagram in Fig. 3a, for a relatively large magnetic flux $\phi = \frac{2\pi}{48}$ for clarity, while the topology of the phase diagram is essentially universal, independent of ϕ. In the $W - E_F$ plane, different QHE plateaus with $\sigma_{xy} = \nu \frac{e^2}{h}$ are separated by extended states, where λ grows linearly with increasing bar width L_y. With the increase of W, each plateau can be destroyed through a transition $\nu \to 0$ to the insulating phase and higher plateaus disappear first. In Fig. 3b-3d, we show examples of calculated localization length to explain how the phase boundaries
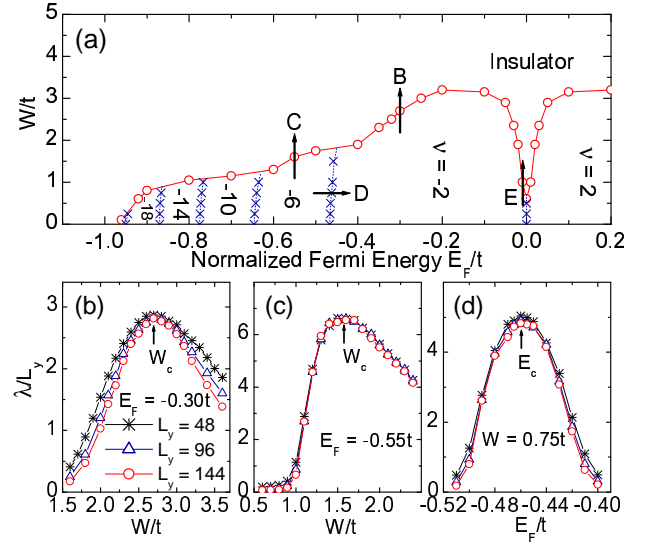

FIG. 3: (a) Phase diagram for the unconventional QHE regime in graphene at $M = 48$, which is symmetric about $E_F = 0$. (b) to (d): Normalized localization lengths calculated for three bar widths $L_y = 48$, 96 and 144, as the phase boundary is crossed by the paths indicated by the arrows B, C and D in (a), respectively.

in the phase diagram are determined. In Fig. 3b, the normalized localization length λ/L_y for $E_F = -0.3t$ and three sample widths $L_y = 48$, 96 and 144 is plotted as a function of W, which corresponds to a $\nu = -2 \to 0$ transition as indicated by the arrow B in the phase diagram. The sample length L_x ranges from 10^6 up to 5×10^6, so that the relative error due to statistical fluctuations in λ reduces to about 2%. We see clearly that λ/L_y is peaked at $W = W_c \simeq 2.7t$, an indication of an extended critical point separating the $\nu = -2$ plateau from the outside insulating phase. Finite-size scaling [17] confirms that the localization length at the thermodynamic limit becomes divergent at W_c. This is consistent with a new "float-up" picture [15], where some negative Chern number states are coming from lower energy, and moving toward the band center with increasing W, which sweep across $E_F = -0.3t$ at $W = W_c$, causing the collapse of the $\nu = -2$ plateau.

Figure 3c shows the normalized localization length as a function of W at $E_F = -0.55t$, corresponding to the path indicated by the arrow C in the phase diagram Fig. 3a. We see that a peak of localization length occurs at $W = W_c \simeq 1.6t$. Similarly to Fig. 3b, the peak indicates the destruction of the $\nu = -6$ QHE state and its transition into the insulating phase. However, we note that here the localization length λ is relatively large, being much greater than the largest L_y that is reachable in our calculations. So λ/L_y does not decrease visibly with increasing L_y, and one cannot rule out a possibility that the higher plateau to insulator transition happens in a critical region with a small finite width ΔW_c instead of
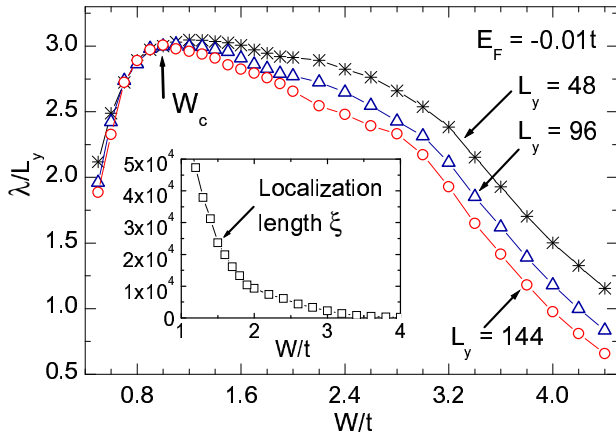
FIG. 4: The normalized localization length λ/L_y for three bar widths $L_y = 48$, 96 and 144, when the phase boundary is crossed with varying disorder strength W at $E_F = -0.01t$, as indicated by the arrow E in Fig. 3a. Inset shows the localization length ξ at the thermodynamic limit determined through one-parameter scaling.

at a critical point W_c, where electron states become delocalized. All the phase boundaries separating the QHE phases from the insulating phase at strong W, indicated by the solid line with open circles in Fig. 3a, are determined in the same way.

To determine the phase boundary between different QHE states, the localization length is calculated as a function of electron Fermi energy E_F for fixed W. As shown in Fig. 3d, corresponding to the path indicated by the arrow D in Fig. 3a, a peak in λ/L_y occurs at $E_F = E_c \simeq -0.46t$, which indicates a critical point separating $\nu = -6$ and -2 plateaus. All the phase boundaries indicated by dotted lines with cross symbols are determined in the same manner.

An important feature of the phase diagram is that the $\nu = -2$ and 2 plateaus around the band center are no longer connected to each other in the presence of disorder, separated by a new insulating phase in between. Corresponding to such a phase transition, along the path indicated by the arrow E in Fig. 3a, we show λ/L_y at $E_F = -0.01t$ as a function of W in Fig. 4. Clearly a largely reduced critical disorder strength $W_c \simeq 1.0t$ is observed in Fig. 4. Following the standard finite-size scaling analysis, we find that all the data in Fig. 4 can be well fitted by a one-parameter scaling relation [17] $\lambda/L_y = f(L_y/\xi)$ for $L_y = 48, 96$ and 144. The fitting parameter $\xi(W)$ is the localization length at the thermodynamic limit. Its value is plotted in the inset of Fig. 4 as a function of W, which becomes divergent at $W_c \simeq 1.0t$. Interestingly, the splitting indicates a singularity in the resistance near $E_F = 0$, as an insulating phase is characterized by a divergent resistance ρ_{xx}, while a plateau state has zero or finite ρ_{xx} (being finite only at the critical point) at low temperature limit. This feature may explain the divergent trend in ρ_{xx} and discontinuity in ρ_{xy}

observed near zero gate voltage in the experiments [6, 7].

We have also confirmed the above phase boundaries by calculating the Thouless number [18], which is proportional to the longitudinal conductance. In particular, we observed that the Thouless number as a function of E_F at fixed W shows two peaks near the band center, while a dip occurs at $E_F = 0$, which is consistent with the splitting of the $\nu = -2$ to 2 transition with a new insulating phase emerging near $E_F = 0$.

In summary, we have numerically investigated the QHE in 2D graphene based upon a lattice model. The experimentally discovered unconventional quantization of QHE is reproduced near the band center, which is understood in terms of the novel distribution of the topological Chern integers in the energy band. The phase diagram indicates a new float-up picture, in which the extended levels move toward band center with increasing disorder strength, causing higher plateaus to disappear first. The unconventional QHE plateaus around the band center are found to be much more stable than the conventional ones near the band edges. A new insulating phase is predicted to emerge at the band center, between two $\nu = \pm 2$ QHE states, which is consistent with the experimentally observed resistance discontinuity near zero gate voltage.

[1] K. S. Novoselov *et al.*, Science **306**, 666 (2004).
[2] C. Berger *et al.*, J. Phys. Chem. B **108**, 19912 (2004).
[3] Y. Zhang, J. P. Small, W. V. Pontius and P. Kim, Appl. Phys. Lett. **86**, 073104 (2005); Y. Zhang, J. P. Small, E. S. Amori and P. Kim, Phys. Rev. Lett. **94**, 176803 (2005).
[4] J. S. Bunch *et al.*, Nano Lett. **5**, 287 (2005).
[5] F. D. M. Haldane, Phys. Rev. Lett. **61**, 2015 (1988).
[6] K. S. Novoselov *et al.*, Nature **438**, 197 (2005).
[7] Y. Zhang, Y.-W. Tan, H. L. Stormer, and Philip Kim, Nature **438**, 201 (2005).
[8] M. Wilson, Physics Today **59**, 21 (2006).
[9] V. P. Gusynin and S. G. Sharapov Phys. Rev. Lett. 95, 146801 (2005).
[10] N. M. R. Peres, F. Guinea and A. H. C. Neto, cond-mat/0506709.
[11] E. McCann and V. I. Fal'ko, cond-mat/0510237.
[12] Y. Zheng and T. Ando, Phys. Rev. B **65**, 245420 (2002).
[13] D. J. Thouless, *et. al.*, Phys. Rev. Lett. **49**, 405 (1982).
[14] L. Sheng, D. N. Sheng, C. S. Ting and F. D. M. Haldane, Phys. Rev. Lett. **95**, 136602 (2005).
[15] D. N. Sheng and Z. Y. Weng, Phys. Rev. Lett. **78**, 318 (1997); D. N. Sheng, Z. Y. Weng and X. G. Wen, Phys. Rev. B **64**, 165317 (2001).
[16] Y. Huo and R. N. Bhatt, Phys. Rev. Lett. **68**, 1375

(1992).

[17] A. MacKinnon and B. Kramer, Phys. Rev. Lett. **47**, 1546 (1981); Z. Phys. B **53**, 1 (1983).

[18] J. T. Edwards and D. J. Thouless, J. Phys. C **5**, 807 (1972).